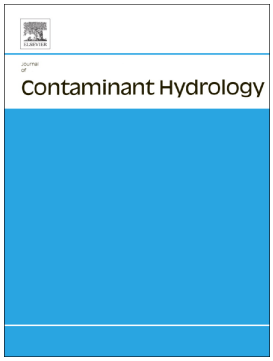

Methane gas transport in unconfined aquifers: A numerical sensitivity study of a controlled release experiment at CFB Borden

Dylan R. Klazinga, Colby M. Steelman, Aaron G. Cahill, Kenneth M. Walton, Anthony L. Endres, Beth L. Parker

PII: S0169-7722(18)30395-4
DOI: https://doi.org/10.1016/j.jconhyd.2019.103506
Article Number: 103506
Reference: CONHYD 103506

To appear in: *Journal of Contaminant Hydrology*

Received date: 7 December 2018
Revised date: 28 May 2019
Accepted date: 28 May 2019

Please cite this article as: D.R. Klazinga, C.M. Steelman, A.G. Cahill, et al., Methane gas transport in unconfined aquifers: A numerical sensitivity study of a controlled release experiment at CFB Borden, Journal of Contaminant Hydrology, https://doi.org/10.1016/j.jconhyd.2019.103506

Methane gas transport in unconfined aquifers: A numerical sensitivity study of a controlled release experiment at CFB Borden

Dylan R. Klazinga[1,2], Colby M. Steelman[1,3,*]cmsteelman@uwaterloo.ca, csteelma@uoguelph.ca, Aaron G. Cahill[4], Kenneth M. Walton[3], Anthony L. Endres[1], Beth L. Parker[3]

[1]Department of Earth and Environmental Sciences, University of Waterloo, Waterloo, Ontario, Canada
[2]Sensors and Software Inc., Mississauga, Ontario, Canada
[3]G[360] Institute for Groundwater Research, College of Engineering and Physical Sciences, University of Guelph, Guelph, Ontario, Canada
[4]Energy and Environment Research Initiative, Department of Earth, Ocean and Atmospheric Science, University of British Columbia, Vancouver, British Columbia, Canada

[*]Corresponding author.

Abstract

Subsurface leakage of natural gas from petroleum wells can impact freshwater aquifers. Accurate prediction of gas migration in the subsurface will depend on knowledge of permeability, porosity, and flow system conditions. A series of two-dimensional numerical multi-phase flow simulations (CFbio) were conducted to investigate the role of multi-phase parameters (relative permeability and air entry pressure), flow system conditions (intrinsic permeability, anisotropy, and groundwater velocity), and geometric properties (layer thickness and layer lateral continuity) on the flow of gas-phase methane emanating from two variable-rate point sources in an unconfined sandy aquifer. Numerical simulations showed that for a homogeneous, weakly anisotropic aquifer, gas migrates almost exclusively vertically due to buoyancy, before venting to the vadose zone and atmosphere. As vertical migration became restricted through increased anisotropy, inclusion of lower-permeable layers, or increased horizontal groundwater velocity, an increase in the lateral component of gas migration was observed. This led to the formation of a broader lateral migration of the gas-phase plume and establishment of variably distributed vertical preferential flow paths, ultimately resulting in increased gas retention in the aquifer with relatively less methane reaching the vadose zone or atmosphere. The inclusion of a thin layer with moderately lower permeability (1–2 orders of magnitude) and increased air entry pressure was used to depict a fine-grained sand lens within a uniform aquifer. This subtle feature led to the formation of thin gas pools extending up- and

down-gradient beneath the lens, allowing methane to travel much farther and faster than by groundwater advection alone, which is consistent with field observations during the experiment. In all scenarios investigated gas-phase methane was shown to migrate predominantly vertically due to buoyancy, until the aquitard permeability was less than 30% of the aquifer permeability. Our modelling demonstrates that even subtle permeability contrasts, together with capillary pressure changes demarcating grain-scale bedding, will lead to extensive lateral free-phase gas migration, and development of a more extensive and complex zone of impacted aquifer than presupposed.

1.0 Introduction

There are several environmental issues associated with hydrocarbon extraction, the understanding of which is a vital step in their mitigation. Hydrocarbon reservoirs are typically formed when a porous host rock is covered by a low permeability layer which traps and prevents the upward migration of buoyant hydrocarbons (Perrodon, 1983). One of the major constituents of trapped hydrocarbons is natural gas comprised primarily of methane, which is becoming of increasing environmental concern with the upsurge in unconventional shale gas development by hydraulic fracturing (Malakoff, 2014). In certain circumstances hydrocarbon extraction wells can release free-phase natural gas into the subsurface leading to groundwater contamination by methane and other higher chain hydrocarbons such as ethane, propane and trace gases (CO_2 and H_2S) (Osborn et al., 2011; Schout et al., 2018; Jackson et al., 2013). In addition, undesirable constituents generated during degradation of methane can degrade groundwater quality (Kelly et al., 1985) while leakage from oil and gas wells can significantly contribute to greenhouse gas emissions (Myhre, 2013). There is a need to understand subsurface gas leakage from a point source such that it can be more effectively monitored, and its potential impacts on groundwater and the environment accurately assessed.

Recent numerical studies aiming to increase understanding of point source methane leakage from hydrocarbon production wells into overlying fresh water aquifers have underscored the importance of multi-phase and multi-component flow system parametrization on the conceptualization of methane transport in the subsurface (e.g., Roy et al., 2016; Moortgat et al., 2018; Rice et al., 2018). Although the potential for methane oxidation exists (e.g., Roy et al., 2016; Schout et al., 2018), much less is known about the mechanisms and controls that influence rapid migration of leaked or fugitive gas and variably scaled dissolved-phase plumes in confined and unconfined shallow aquifers. Moortgat et al. (2018) illustrated the importance of injection rate, preferential pathways, and optimal layer geometry to facilitate lateral gas migration on the evolution of methane plumes specifically along fractures or channels in bedrock formations. Rice et al. (2018) showed the relative importance of air-entry pressure and relative permeability parameters in developing an accurate conceptual model of methane gas migration through a low-permeability unfractured medium. Subsequently they showed variations in gas-phase pressure and saturation would significantly impact the flow rate of methane entering a freshwater aquifer; however, the evolution of the methane plume toward a freshwater aquifer would be primarily controlled by the intrinsic permeability of the medium and the source zone pressure.

A controlled methane injection field experiment was conducted at Canadian Forces Base (CFB) Borden to evaluate the migration of free-phase methane in an unconfined sandy aquifer (Cahill et al., 2017) and its impact on groundwater chemistry (Cahill et al., 2018). Over a period of 72 days, 51.35 m^3 was injected into the aquifer at two depths: 4.5 and 9.0 mbgs. The migration of methane was characterized using high-resolution multi-level groundwater geochemical and microbial sampling, surface electrical resistivity and ground-penetrating radar, vadose zone and surface gas efflux measurements (Steelman et al., 2017; Cahill et al., 2018; Forde et al., 2018).

Initial estimates indicated that approximately half of the gas quickly vented to the atmosphere (days to weeks after the start of the injection), while the other half remained in the groundwater for an extended period (weeks to months) (Cahill et al., 2017). Despite the growth of methanotrophic bacteria below the water table, dissolved methane persisted in the groundwater at levels of concern (i.e. >10 mg/l) (Eltschlager et al., 2001), while a significant amount of free-phase gas that vented into the vadose zone was oxidized (Forde et al., 2018). Using a network of multi-level monitoring wells, depth-discrete groundwater samples for dissolved gases were collected before, during and after the active injection period (Cahill et al., 2017). At the Borden site, it was shown that after entering the aquifer, free-phase methane gas preferentially migrated upward due to buoyancy while a nearly equal portion migrated laterally due to subtle grain-scale bedding (Cahill et al., 2017). Free-phase gas migration was attributed as the dominant factor controlling the lateral extent of the dissolved phase plume, contributing to a more extensive dissolved methane plume than that based solely on advective groundwater flow. Results also suggested that dewatered gas migration channels were established during active gas inflow into the aquifer, which facilitated more rapid transfer of methane to the vadose zone, thus limiting potential mass transfer between gaseous and aqueous phases. This process led to moderately elevated dissolved hydrocarbon gas concentrations in the aquifer (approximately half the theoretical solubility limit, as calculated using mole fractions of injected gas constituents, based on Dalton's Law). Once gas inflow ceased and pressures dropped, these channels most likely collapsed resulting in re-saturation of pore spaces, increasing gas-water mixing, and increased levels of dissolved hydrocarbon gases approaching theoretical solubility limits (Cahill et al., 2018). This behaviour ultimately led to a persistent dissolved methane plume 323 days after the injection was terminated, whereby dissolved methane and stable carbon isotopes showed

minimal signs of microbial-mediated degradation. Overall, the field experiment demonstrated that fugitive gas will be highly mobile in groundwater, particularly during a pressurized leakage state. Under such conditions fugitive gas exhibits a propensity to migrate substantial lateral distances controlled by small-scale sediment layering and anisotropy, creating laterally extensive and complex dissolved gas plumes which can persist for years due to apparently low rates of degradation.

Although Cahill et al. (2017) was able to observe and characterize gas migration from a point source leak in an unconfined aquifer, the physical conditions controlling that migration were not fully understood. To evaluate the physical interactions inherent in this process-based conceptualization of gas migration in an unconfined aquifer, we have conducted a systematic numerical modelling study to evaluate how permeability, anisotropy, stratigraphic boundaries, gas entry pressure, groundwater velocity, injection rate history, and overall experimental design impacted the migration and storage of free-phase methane during the controlled release experiment at CFB Borden. This was achieved by defining a basic two-dimensional (2D) flow model scenario, and systematically adjusting model parameters to produce a range of flow system scenarios stylistically informed by the methane injection field experiment observations (Cahill et al., 2017; Steelman et al., 2018; Forde et al., 2018) as well as from decades of groundwater research at CFB Borden (Sudicky and Illman, 2011). This systematic approach captures increasing degrees of physical complexity in Borden aquifer properties believed to be contributing to the observed evolution in the gas-phase plume. Numerical results are used to elucidate the primary physical controls and their interactions influencing the establishment of vertical preferential pathways to the vadose zone, gas-phase distribution over time, and potential longer-term storage within the unconfined groundwater flow system. Our numerical simulations

assume a non-reactive and relatively insoluble gas impeded by a single low-permeable layer under varying hydraulic properties and conditions, and that general gas plume behaviour can be adequately represented through a 2D model.

2.0 Methods

2.1 Multi-Phase Flow Simulations

Although the Borden sand is relatively homogeneous for saturated flow conditions, subtle changes in grain-scale bedding (Thomson, 2004) can contribute to marked heterogeneity in multi-phase flow properties (Tomlinson et al., 2003). Rather than attempt to replicate centimetre-scaled heterogeneity, a more simplistic approach was adopted based on these insights. The objective of this study was to conduct a systematic sensitivity analysis of the methane injection field study to assess the experiment design (rather than attempting to replicate results) by Cahill et al. (2017) and determine pertinent hydrological parameters and field conditions contributing to the observed evolution of the methane gas plume. Our approach described herein provided better control on model parameter sensitivity to transport characteristics of methane gas migration in an unconfined aquifer, ultimately gaining clearer insights on the relative importance of individual flow system properties and site conditions on methane gas migration in the subsurface observed during the complementary controlled release experiment initially reported by Cahill et al. (2017).

Our 2D conceptual model of the Borden aquifer consists of an unconfined aquifer over an aquitard (Figure 1). Since the primary objective of this study was to understand the relative importance of hydraulic properties, aquifer conditions, and overall experimental design on the lateral migration of the methane gas plume, our 2D models are assumed to be reasonable representations of the true three-dimensional system. A base case conceptual model was

informed by continuous core retrieved at the CFB Borden methane injection site (Cahill et al., 2018). Falling head permeameter measurements of repacked soil samples from the soil core revealed a four-layer system (Steelman et al., 2017). The first three layers were dominated by fine to coarse sands (94 – 99%) with high permeability within the same order of magnitude ($k \approx 1\times10^{-12}$ m^2). The fourth layer, beginning at a depth of approximately 7.4 m, identified the gradual transition into aquitard and was accompanied by progressively higher percentages of silts and clays (17 %) with a permeability $k \approx 1\times10^{-14}$ m^2.

The first layer in the model (Figure 1) represents an amalgamation of the upper three layers delineated by the permeameter measurements and was represented by an average lateral permeability (k_h) of 2.2×10^{-12} m^2 and a porosity (ϕ) of 0.33. The second layer in the model represents the aquitard, $k_h = 6.4\times10^{-14}$ m^2 and $\phi = 0.39$. Permeability ranges were based on the permeameter measurements of the repacked soil samples from the actual injection site (Steelman et al., 2017). Literature values for porosity of the Borden sand were used for these models (Das, 2008). The boundary between the aquitard and the aquifer was set at 9.0 m bgs; both the aquifer and aquitard anisotropy ratio (k_h/k_v) was set to 10. An anisotropy ratio of 10 is consistent with observed and simulated conservative tracer studies in the Borden aquifer. The Borden aquifer can be described as an assemblage of near-horizontal beds of contrasting hydraulic conductivity with thicknesses of a few centimeters to a few tens of centimeters. Given the discontinuous nature of these beds, they have been stylistically defined in this study by establishing an anisotropic system that would otherwise be considered a homogeneous environment (Sudicky, 1986).

The boundary conditions were set to maintain a 1.0 m depth to the water table directly above the injectors at 4.5 and 9.0 m bgs with a steady ambient groundwater flow from left to right,

atmospheric gas exchange, and recharge (Figure 1). Pressures of 189 kPa and 187 kPa are assigned at the left and right bottom corners, respectively, to set the hydrostatic conditions on the vertical boundaries and create a gradient along the bottom. The upper boundary, representing the atmosphere, was defined by a pressure of 100 kPa. Recharge was applied in the second grid layer at a constant rate of 0.7 mm/day. The model was initialized as fully saturated below a depth of 0.7 m bgs with 60% saturation above 0.7 m bgs and was allowed to equilibrate for 100 days prior to the start of the injection.

The pressure at which imbibition occurs is called the air-entry pressure ($P_{c\ entry}$) and is a characteristic of the pore geometry (Fetter, 1992). Leverett (1940) established that the capillary pressure (P_c) is proportional to the squared inverse of the hydraulic permeability. When the pressure exceeds the air-entry pressure the material will desaturate, asymptotically approaching the residual saturation (Brooks and Corey (1964):

$$S_e = \frac{S - S_r}{1 - S_r} = \frac{\theta - \theta_r}{\phi - \theta_r} = \left(\frac{P}{P_c}\right)^{-\lambda}, \quad [1]$$

where S_e is effective saturation (-), S is saturation (-), S_r is residual saturation (-), θ_r is residual volumetric water content (-), ϕ is porosity, P is pressure of the non-wetting phase (N/m^2), and λ is the Brooks-Corey parameter (-), which is a property of the medium. As desaturation occurs, the relative hydraulic permeability for the pore fluid decreases. Using the Brooks-Corey model (Brooks and Corey, 1964), the relative permeability for the wetting (k_{rw}) and non-wetting phase (k_{rnw}) can be calculated by:

$$k_{rw} = \left(\frac{P}{P_c}\right)^{-(2+3\lambda)} \quad \text{for } P \geq P_c \qquad [2a]$$

$$k_{rnw} = \left[1 - \left(\frac{P}{P_c}\right)^{-\lambda}\right]\left[1 - \left(\frac{P}{P_c}\right)^{-(2+\lambda)}\right] \quad \text{for } P \geq P_c \ . \qquad [2b]$$

Relative permeability was determined using the Brooks-Corey parameters for the Borden aquifer from Kueper and Frind (1991), where P_c = 2.22 kPa, θ_r = 0.078, and λ = 2.48. A residual gas saturation of 10% was assumed. Our free-phase flow modelling assumes no methane degradation over the relatively short time-scale of the active injection phase (i.e., 72-day injection period); this simplification is supported by stable carbon isotope analysis (Cahill et al., 2018). Additionally, the influence of temperature, variations in precipitation, evapotranspiration, and barometric pressure dynamics were not considered in the scope of this paper.

The injector geometry was modelled after the actual injector setup (Cahill et al., 2017). Gas injectors were placed at 4.5 m and 9.0 m bgs, 8 m from the up-gradient boundary. A four-stage stepped injection rate was used: a slow injection rate (Phase I: 2 × 0.06 L/min), a moderate injection rate (Phase II: 2 × 0.35 L/min), a moderate injection from the deeper well only (Phase III: 1 × 0.35 L/min), and a fast injection (Phase IV: 2 × 1.5 L/min) (Figure 2). This simulated injection scenario follows the reported injection rates by Cahill et al. (2017) (Table 1). A temporary shutdown of the injectors was also simulated during Phase II between Days 38 – 44 as per the field experiment. Each injector was modelled as a point source during Phases I – III, while a slightly more distributed injector (0.3 m high and 0.2 m wide) was used during Phase IV to reduce risk of model instability during the otherwise instantaneous transition to the highest injection rate (Phase IV).

2.2 Numerical Model and Parametrization

CompFlowBio (CFbio) (Forsyth and Shao, 1991; Unger et al., 1995) was selected to complete the methane flow numerical modelling. The model simulates flow and transport of three mobile

phases (aqueous, non-aqueous, and gas) for various components (methane, water, and air in this study) with equilibrium phase partitioning. CFbio uses a fully implicit, first-order accurate, finite-volume spatial and temporal discretization scheme and adaptive time stepping. Convergence properties of the discretization scheme have been demonstrated in Walton et al (2017 and 2018), albeit for water-NAPL flow in fractured porous rock. The set of coupled, non-linear governing partial differential equations for pressure, and conservation of mass (via phase saturation and mole fraction) are solved using Newton-Raphson iteration. The CGStab acceleration scheme is employed by the solver.

A model domain of 10 m high by 20 m long, and 0.1 × 0.1 m discretization was used for all simulations presented herein, despite many other configurations explored during development. A height of 10 m was used as a negligible pressure response during injection was observed 1 m below the top of the aquitard; domain length and spatial discretization were chosen to maintain simulation tractability and mitigate boundary condition effects during Phases I – III. For Newton iteration, the convergence tolerances were 1×10^{-4} kPa for pressure, 1×10^{-5} for saturation, 1×10^{-7} for the mole fraction of methane. During Phase IV, the highest injection rate made it difficult for CFbio to converge, so the tolerances were relaxed to 5×10^{-3} kPa, 5×10^{-4}, and 5×10^{-6}, respectively. Gas saturation, particularly at the edge of the plume where new control volumes were being invaded, exhibited some sensitivity to discretization and tolerance values, yielding slightly different phase architectures for otherwise similar runs. Subtle differences in pressure and mole fraction (phase composition and density) lead to buoyancy differences and gravitational instabilities in the phase front, while saturation differences yielded instabilities in phase mobility. These ultimately represent limitations of our numerical model. A formal investigation of grid convergence and numerical sensitivity is beyond the scope of this paper.

Therefore, the simulations presented herein specifically address only our present goal of examining parameter sensitivity at a coarser, simulation design-type level.

2.3 Modelled Scenarios

The base scenario was modified to investigate the sensitivity of hydraulic properties, layer geometries, and flow system conditions on the spatiotemporal evolution of a free-gas plume generated from a 72-day methane injection followed by a 30-day recovery period (102-day simulated period) in the unconfined sandy aquifer. The physical properties used to define the basic model scenario and sensitivity analysis is provided in Table 2. A summary of the model scenarios considered in this study is provided in Table 3. All physical parameters and modelled ranges were based on literature values for the Borden aquifer and field measurements collected at the experimental test site.

Permeability

The influence of subtle permeability contrasts in the aquifer was investigated through the addition of a macroscopic continuous layer in the subsurface. A layer of finite thickness was added from 3.0 – 3.5 m bgs with $\phi = 0.33$ equal to that of the adjacent aquifer material. A range of permeability contrasts were considered to relate the homogeneous permeability of the layer, k_L, to the permeability of the aquifer, $k_{aq} = 2.2 \times 10^{-12}$ m^2: $k_L = 1 \times k_{aq}$, $k_L = 0.55 \times k_{aq}$, $k_L = 0.3 \times k_{aq}$, $k_L = 0.1 \times k_{aq}$, and $k_L = 0.03 \times k_{aq}$. For all scenarios the entry pressure and porosity of the layer was equal to that of the aquifer: $P_c = 2.22$ kPa and $\phi = 0.33$.

Anisotropy

To assess the impact of anisotropy on the flow of methane the base case was modified using a range of anisotropy ratios. The horizontal hydraulic permeability (k_h) of the aquifer and aquitard were fixed, having the same value as in the base case (i.e., k_L and k_{aq}), while the vertical hydraulic permeability was adjusted to create the desired anisotropy ratio. The following anisotropy ratios were considered: $k_h/k_v = 5$, $k_h/k_v = 10$, and $k_h/k_v = 30$. These three cases were then repeated with a layer added within the aquifer from 3.0 m – 3.5 m bgs, with $k_L = 0.1 \times k_{aq}$ and $\phi = 0.33$. This range in anisotropy is consistent with reported values of k_h and k_v for Borden sand (Sudicky, 1986).

Groundwater Velocity

One scenario was used to examine the impact of groundwater velocity on the flow of methane; the base case was run with a range of different boundary pressure conditions to produce the desired groundwater flow velocity across the model domain while maintaining a fixed depth of 1.0 m to the water table directly above the injectors. The aquifer permeability was $k_{aq} = 2.2 \times 10^{-12}$ m^2 and $\phi = 0.33$ with an anisotropy ratio of $k_h/k_v = 10$. Four different groundwater velocities were modelled: 0 cm/day, 3 cm/day, 6 cm/day, and 10 cm/day. These flow rates corresponded to horizontal hydraulic gradients of 0 m/m, 0.00449 m/m, 0.0106 m/m, and 0.0177 m/m, respectively.

Layer Thickness

One scenario was used to assess the impact of the layer thickness on the flow of free-phase methane: an equivalently anisotropic layer with $k_L = 0.55 \times k_{aq}$ and $\phi = 0.33$ was added to the subsurface. The top of the layer was maintained at a depth of 3.0 m bgs while the depth to the

base of the layer was adjusted to give the desired layer thickness. Three layer thicknesses were considered: 0.2 m, 0.5 m, and 1.0 m.

Entry Pressure

The impact of entry pressure on the flow of methane gas was assessed through two scenarios. In the first scenario a layer from 3.0 – 3.5 m bgs was added to the base case with $k_L = 0.55 \times k_{aq}$ and $\phi = 0.33$. This was modelled twice, once with the layer entry pressure equal to the aquifer (i.e., $P_c = 2.22$ kPa) and once with the entry pressure of the layer increased to $P_c = 2.99$ kPa; here, the entry pressure of the layer was scaled according to its permeability (Leverett, 1940).

Layer Discontinuity

The role of a discontinuity along a lower-permeable layer was evaluated for the case of a layer from 3.0 – 3.5 m bgs with $k_L = 0.55 \times k_{aq,}$ $\phi = 0.33$ and $P_c = 2.99$ kPa. Three simulations were run placing a 1 m wide discontinuity within the layer centred at three different positions up- and down-gradient of the injection points (i.e., -1.5 m, 2.5 m and 6.5 m, relative to the position of the injectors).

Injection History

To assess the impact of injection history (i.e., using a stepped injection rate during the field experiment) on the flow of methane gas in the aquifer, three simplified injection scenarios were considered, which were based on a fixed rate at each injector for the full 72-day injection period: 0.06 L/min, 0.35 L/min, and 1.50 L/min. These three scenarios were compared to the stepped injection rate scenario. All scenarios included a layer from 3.0 m – 3.5 m, with $k_L = 2.2 \times 10^{-13}$ m^2 and $\phi = 0.33$ with no change in entry pressure.

Injector Configuration

The implication of injecting gas simultaneously at two depths in the aquifer (i.e., 4.5 and 9.0 m bgs) was evaluated through a comparison of gas plume migration associated with individual injection scenarios. In this case, a uniform aquifer with no layer and a constant stepped injection rate history was used.

3.0 Results and Discussion

3.1 Permeability

The base case of methane gas injection into a uniform aquifer (i.e., $k_L = 1 \times k_{aq}$; Figure 3a) showed that the gas-phase migrated upward under buoyancy. As the gas migrated toward the water table, it spread horizontally creating a plume that was thin near the source and wide where it vented into the vadose zone (gas-phase distribution for Day 56 of the base case injection is presented in Figure 3a). The plume was slightly skewed in the direction of groundwater flow, extending farther down-gradient than up-gradient. The plume geometry shows the dominant role of buoyancy and pressure gradients in methane migration. The gas migrates upwards once the pressure gradients and buoyant forces exceed the hydrostatic pressure of the overlying water column; lateral spreading is enhanced by increased pressure (i.e., injection rate). These results are consistent with those of previously reported air-sparging modelling studies (Thomson and Johnson, 2000).

The effects of a lower permeability layer were evaluated with four different layer permeability (k_L) values relative to the background aquifer permeability ($k_{aq} = 2.2 \times 10^{-12}$ m^2): $k_L = 0.55 \times k_{aq}$, $k_L = 0.3 \times k_{aq}$, $k_L = 0.1 \times k_{aq}$, and $k_L = 0.03 \times k_{aq}$. These scaled permeabilities were considered with a uniform porosity of $\phi = 0.33$ across the aquifer and neglected any associated

changes in air-entry pressure. Although air-entry pressure is inversely associated with permeability, this section specifically considers the role of permeability on the retention and accumulation of gas in the aquifer without the added effects of capillary pressure on gas-phase (the influence of air-entry pressure on gas migration will be examined in Section 3.5).

Results from Day 56 (Figure 3a) show that a decrease in layer permeability will enhance lateral migration of the methane gas and distribution of efflux at the water table interface. As migrating through the layer to the vadose zone becomes more difficult, more gas migrates laterally to relieve the pressure of the plume below the layer. In the cases of lower permeability contrast (e.g., $k_L \geq 0.3 \times k_{aq}$), the highest gas saturations formed between the shallow injector and the water table with minimal resistance to vertical flow from the layer, enabling the formation of a preferential gas pathway where gas migrates more rapidly to the vadose zone, and thus formation of gas hotspots (i.e., zones of relatively higher gas phase saturation) along the water table interface. For conditions with higher layer permeability contrast (e.g., $k_L \leq 0.1 \times k_{aq}$) methane emission to the vadose zone was more dispersed, preferentially accumulating gas below the layer. Thomson (2004) drew similar conclusions from cores taken at a contaminated site at CFB Borden, where dense non-aqueous phase liquids (DNAPLs) would preferentially pool at permeability contrasts.

The simulations showed that at early time (e.g., Day 1) the gas from the shallow injector was more mobile owing to the lower hydrostatic pressure, migrating vertically to the vadose zone more quickly (within the first 24 hours) compared to the deeper injector for both uniform and layered cases. As the gas injection proceeded (e.g., Days 20 – 71) the lower permeability layer enhanced lateral migration in both the up- and down-gradient direction with consistently higher gas saturations within and below the layer relative to the uniform case. At lower injection

rates (i.e., Phases I – III; Days 0 – 70), the gas would spread up- and down-gradient along the base of the layer before migrating vertically through the layer toward the vadose zone. At higher injection rates (i.e., Phase IV; Day 70 – 72), the gas further expanded along the base but did not establish a clear preferential pathway vertically to the vadose zone. During the late stages of the injection, the highest gas saturations were observed along the edges of the methane plume below the layer. Following the cessation of the injection on Day 72, residual gas saturation values were similar in both the uniform and layered cases, however the spatial extent of these residual conditions was greater (>3 time) for the layered cases.

These results show the influence of the shallow injector location on the distribution of gas emanating from the deeper injector. Here, increased hydrostatic pressures associated with the simultaneous injection from a shallow and deep point led to the formation of a thin gas lens approximately 1 m above the deep injector. This small gas lens widened with decreasing layer permeably, increasing injection rate, and increasing anisotropy ratio. Under higher anisotropic conditions (i.e., $k_h/k_v = 30$) the gas emanating from the deep injector partitions between two vertical migration pathways located up- and down-gradient the injection horizon. This effect is further evident in the absence of gas along a thin column between the shallow and deep injector, which facilitated the formation of multiple gas hotpots at the water table interface.

The volume of methane gas contained in the subsurface (Figure 3b) was always higher in the case with a layer during the 102-day simulation period. Gas retention in the aquifer varied with injection rate. During Phase I (Days 0 – 28) of the injection, there was only a marginal increase in gas retention with the inclusion of a lower permeability layer (e.g., $k_L = 0.55 \times k_{aq}$ retained ~7% more gas compared to the uniform case). Following the cessation of the injection, more gas remained in the subsurface of the layered cases (i.e., up to ~28% for $k_L = 0.1 \times k_{aq}$ on Day 102),

which is consistent with the enhanced lateral spreading and higher gas saturations observed below the layer and shown in Figure 3a.

The volume of gas in the subsurface changes rapidly following a rate change; but as time progresses, the rate of change of gas volume in the subsurface eventually slowed, reaching a steady-state condition. This response implies that once a preferential path is established, the system will reach equilibrium unless it is perturbed. The addition of a layer facilitates gas phase mixing as demonstrated by the mixing of the shallow and deep plumes in our simulations. As the pressure required to push gas through the low-permeable zones increases, a portion of the gas will inevitably spread within and below that zone, resulting in much wider plumes than observed within relatively more permeable formations or those lacking lower permeable interbeds. These wider plumes will also be accompanied by higher gas retention in the aquifer which would have implications for potential chemical reactions or methane degradation. During the field experiment, Cahill et al. (2017) noted that approximately half of the methane injected into the aquifer quickly vented to the atmosphere, while the other half remained in the subsurface for an extended period. These observations, coupled with these simulations, suggest that the methane retained in the aquifer migrates laterally significant distances where it would remain until degradation occurs.

3.2 Anisotropy

Six cases with varying anisotropy ratio were considered: $k_h/k_v = 5$, $k_h/k_v = 10$, and $k_h/k_v = 30$ for a uniform aquifer and for an aquifer with a lower permeability layer ($k_L = 0.1 \times k_{aq}$, $\phi = 0.33$) (Figure 4). Each simulation was performed using a horizontal aquifer permeability of $k_h = 2.2 \times 10^{-12}$ m^2. On Day 56 (Figure 4a) the gas travelled upwards and spread laterally in the up- and down-gradient directions along the water table surface. Lateral spreading increased with

anisotropy, creating a wider zone of desaturation. In the cases with lower anisotropy ratios (e.g., $k_h/k_v = 5$) and a uniform aquifer, the methane plumes from both injectors mixed readily due to dominantly vertical flow paths, forming a focused gas hotspot above the injectors at the water table. For the cases with higher anisotropy ratios (e.g., $k_h/k_v = 30$) and a uniform aquifer, the gas plumes from both injectors experienced greater separation resulting in a more heterogeneous gas distribution. This distribution ultimately led to the early formation of two hotspots: one slightly up-gradient, above the shallow injector and another farther down-gradient emanating from the deeper injector. The presence of a lower-permeability layer systematically enhanced lateral spreading and dampened the concentration of methane gas hotspots at the water table.

Enhanced spreading and lateral migration with increasing anisotropy (i.e., decreasing vertical permeability) resulted in higher gas volumes in the aquifer during the active injection phase (up to 10 m^3 on Day 72; Figure 4b). This increase in gas retention can be explained by the plume width increasing with the degree of anisotropy and the additional migration time. The additional size of the methane gas plume, despite being at a lower gas saturation above the layer, increases the volume of gas retained in the subsurface after the injection ceases. Additionally, more time was required for the cases with higher anisotropy ratios to reach steady-state conditions during active injection and to reach the residual gas saturation after the injection was terminated on Day 72.

Similar to adjusting the permeability within the layer, changing anisotropy affects where the greatest water desaturation will occur. At low anisotropy, gas preferentially accumulates within the layer, whereas with higher anisotropy gas remains below the layer. These two responses are similar to gas behaviour when a layer in the aquifer has a low permeability contrast (i.e., $k_L \leq 0.3 \times k_{aq}$) or a high permeability contrast (i.e., $k_L \geq 0.1 \times k_{aq}$), respectively. The division between

these two accumulation patterns appears to relate to the ratio of the vertical component of permeability to the horizontal component of permeability in the formation above, with a high contrast layer (i.e., gas preferentially accumulating below a layer) being defined by a vertical permeability two orders of magnitude less than the lateral permeability of the adjacent formation.

3.3 Groundwater Velocity

A uniform aquifer scenario was modelled with varying average linear groundwater velocity: 0 cm/day, 3 cm/day, 6 cm/day, and 10 cm/day (Figure 5). In the absence of groundwater flow (i.e., zero hydraulic gradient), a relatively symmetric chimney formed directly above the injectors leading to rapid gas migration to the vadose zone and the formation of a hotspot at the water table (Figure 5a). This behaviour aligns with the results of Thomson and Johnson (2000), whose modelling of air-sparging at CFB Borden showed the formation of a symmetric chimney that spread in width as the gas migrated vertically. With the inclusion of horizontal groundwater flow, the gas preferentially migrated down-gradient; the degree of down-gradient migration increased with groundwater velocity. Increasing the groundwater velocity eventually led to the formation of two distinct gas plumes (e.g., 10 cm/day), each emanating from their source of origin.

Horizontal groundwater flow enhanced lateral migration, smearing the gas plume across a larger area of the aquifer, increasing the gas retention by up to ~20% (Day 72; Figure 5b). Interestingly, the increase in gas retention in the model domain is non-linear with respect to the groundwater velocity, with negligible increase in the volume of gas between the 3 cm/day and 6 cm/day cases relative to the increases observed between the 0 cm/day and 3 cm/day cases and the 6 cm/day and 10 cm/day cases. The non-linearity of methane gas retention is likely related to plume

separation (i.e., alteration in the position of preferential pathways with respect to injector geometry and hydraulic gradients).

When there is no groundwater flow, the pathway of gas migration forms a single compact channel with the gas rising from the deeper injector more quickly due to the sudden reduction in the hydrostatic pressure caused by the upper injector. When the groundwater is flowing, the gas pathways are pushed farther down-gradient such that the effects of overlying hydraulic pressure (i.e., the cumulative contribution of the shallow injector on the deeper injector gas emission) are lower. Since the gas is no longer migrating in a vertical path, a longer path, with a higher volume is needed to connect the gas from the deep injector to the gas plume from the shallow injector. The length of this path is not changed considerably when the groundwater velocity increases from 3 cm/day to 6 cm/day since the plumes from both injectors still eventually combine to form a single pathway. Increasing the groundwater velocity further shifts the position of the plume from the deep injector until the plumes no longer converge. This divergence led to a marked increase in gas retention (i.e., the increase observed between 6 cm/day and 10 cm/day), since the two individual pathways contain more gas than a single shared pathway.

3.4 Layer Thickness

A layer with $k_L = 0.55 \times k_{aq}$ with an upper boundary at a depth of 3 m bgs was added to the aquifer ($k_{aq} = 2.2 \times 10^{-12}$ m^2, $\phi = 0.33$) for three different layer thicknesses: 0.20 m, 0.50 m, and 1.00 m. Conditions on Day 56 (Figure 6a) reveal increased lateral spreading up- and down-gradient with increasing layer thickness. This lateral spreading was accompanied by a systematic reduction in the magnitude of gas saturation above the layer, resulting in a more diffuse gas distribution along the water table interface (i.e., defocussing hotspot). Gas retention in the

aquifer (Figure 6b) increased non-linearly with layer thickness. A more notable difference in gas volume was observed at moderate and higher injection rates (i.e., Phases II – IV) with more gas retained in the aquifer for progressively thicker layers (up to ~36% more gas in aquifer on Day 48).

3.5 Entry Pressure

The effect of layer entry pressure was considered for the case of an aquifer with a layer from 3.0 m – 3.5 m bgs with $k_L = 0.55 \times k_{aq}$ for two air-entry pressure scenarios: P_c = 2.22 kPa representing the case of a uniform entry pressure across the layer boundary; and P_c = 2.99 kPa representing the case of an increase in gas entry pressure of the less permeable layer (Figure 7a).An increase in the entry pressure of the layer relative to the adjacent material resulted in free-phase gas pooling along the lower boundary of the internal layer. This pooling led to an increase in pore pressure along the interface, which eventually led to imbibition of gas into the layer, which resulted in the formation of distinct vertical preferential pathways up- and down-gradient from the injection points that progressively widened as the injection commenced. Although an increase in gas entry pressure enhanced the spatial distribution of the gas below the layer, a negligible increase in overall plume width was observed above. However, gas efflux into the vadose zone was more variably distributed for the higher entry pressure scenario, resulting in the formation of multiple gas hotspots into the vadose zone.

Even though changes in layer entry pressure contributed to more variable distributions of gas within the aquifer, it had a minor impact on the volume of gas retained in the aquifer (<5%; Figure 7b). Here, the slight differences in gas retention between the case with and without adjusted entry pressures are likely attributed to the formation of additional pathways through the low permeability layer. A closer inspection of the volume of gas within the aquifer for the two

entry pressure cases reveals that the volume of gas retained is not simply associated with changes in gas-entry pressure.

As the gas migrated vertically towards the low-permeable layer with a higher entry pressure (P_c = 2.99 kPa) it spread more quickly along the base of the layer and travelled much farther than along the interface compared to the case with no change in gas-entry pressure. The migration occurred in a relatively thin pool of gas that formed as a distinct lens under the layer. From this pool thin paths broke through the layer and travelled upwards eventually venting to the vadose zone. All these thin features that made up the migration pathways of the gas-phase methane created a distribution of gas much more heterogeneous than seen in the unadjusted cases. This pattern of migration is similar to observations, in an inverse manner, to Brewster et al. (1995) with DNAPLs settling on top of less permeable lenses. The authors showed that dense fluids travelling downwards due to gravity would settle on top of the low-permeable lenses eventually breaking through as the DNAPL accumulated forming preferential pathways through the layer.

Cahill et al. (2017) made several observations consistent with the numerical simulations of gas migration for the case of a layer with increased entry pressure. The first observation was the occurrence of variable methane efflux patterns at the surface. Cahill et al. (2017) began noting methane efflux hours after the beginning of the injection at isolated locations (~5 m^2), which agrees with the conceptual model of dominant vertical migration caused by buoyancy together with the formation of preferential channels caused by variations in gas entry pressure. The zones from which the gas escaped to the atmosphere were on the order of a few meters in the field experiment, which again, is consistent with the modelling in this study. Therefore, gas efflux zones are likely to be more concentrated in cases where the aquifer contains layers with subtle differences in layer entry pressure. The temporal efflux patterns observed during the field

experiment were different than depicted in these simulations. Forde et al. (2018) reported multiple episodic release events at various locations around the injectors that fluctuated in magnitude (i.e., daily emissions of 38 – 261% gas injected over that time), while our modelling shows a more consistent venting that changes with injection rate. This difference could be attributable to the inherent qualities of increased heterogeneity and external forces acting upon groundwater flow inherent to real hydrologic systems. For example, the transience observed during the field experiment could be explained, in part, by barometric or hydraulic pressure variations, or most likely by gas building-up and releasing in multiple interconnected or cascading lenses in the aquifer.

3.6 Layer Discontinuity

Three cases were modelled where the lower-permeable layer did not extend across the entire width of the model domain. Each scenario consisted of a layer with a 1 m wide discontinuity centered at -1.5, 2.5 and 6.5 m, relative to the injectors. The layer was placed from 3.0 m – 3.5 m bgs with $k_L = 0.55 \times k_{aq}$, $\phi = 0.33$, and $P_c = 2.99$ kPa. Based on the change in gas saturation relative to the start of the injection on Day 56 (Figure 8a), layer discontinuities resulted in a notable impact on the timing and position of the hotspot arriving at the vadose zone. Slight variations in the positioning of the discontinuity had a marked effect on the distribution of the gas phase within the aquifer. As the discontinuity was shifted farther down-gradient (e.g., 6 m to 7 m) there was diminished influence on the positioning of the gas plume; however, the distribution of low saturation regions became more variable as shown by the formation of multiple vertical pathways up- and down-gradient.

The relative impact of a layer discontinuity on the volume of gas retained in the aquifer was subtler. At low leakage rates (Phase 1) the total volume of gas in the aquifer was largely the

same for the three discontinuity cases. As the injection rates increased (Phase II – IV) there were more notable differences in gas accumulation (up to 7%; Figure 8b), with the up-gradient discontinuity resulting in consistently lower gas retention compared to both down-gradient discontinuities. Interestingly, both down-gradient cases resulted in very similar gas retentions, with only slightly higher gas volumes for the farthest down-gradient case.

3.7 Injection Rate History

Four cases were used to assess the impact of the injection rate history: two cases using the actual injection rate (Figure 2; Table 1), and three cases based on a single constant injection rate corresponding to the individual rate steps: Phase I (0.06 L/min), II (0.35 L/min), and IV (1.50 L/min). Each injection rate was modelled with a uniform aquifer ($k_{aq} = 2.2 \times 10^{-12}$ m^2, $\phi = 0.33$) with a layer placed between 3.0 and 3.5 mbgs ($k_L = 0.55 \times k_{aq}$). Higher injection rates led to greater gas retention in the aquifer and lateral migration in both the up- and down-gradient direction and higher levels of water desaturation (gas saturation plots not shown). The gas plume characteristics drawn from the actual injection rate largely resembled an amalgamation of each of the individual rates: low gas saturations above the layer resembled that of the lowest injection rate case; the broad lateral extent of the plume was consistent with that of the moderate injection rate; and the extensive desaturation and pooling of gas beneath the layer was similar to that observed at the highest injection rate.

The gas retention curves suggest more variable gas residence times for the actual injection history case compared to the constant rate injection scenarios (Figure 9). An examination of the total gas in the subsurface during Phase II, before and after the temporary shut-down, reveals differences in gas saturation related to the effects of the previous gas imbibition episode. For

instance, the temporary shut-down results in residual gas that initially impedes the vertical migration of the gas plume once the injection is reinitiated, therefore causing the plume to spread over a larger footprint than it did prior to the shutdown. This resulted in a temporary increase in gas storage within the aquifer following the shut-down. As Phase II injection advanced, the gas eventually re-established pathways to the vadose zone and reached steady-state conditions. Therefore, the stepped injection rate history combined with an abrupt shut-down led to variable gas residuals within the aquifer, contributing to more variable gas-phase behaviour compared to a single constant injection rate.

These simulations suggest that gas residence can be associated with changes in injection rate. Observations during the field experiment revealed numerous episodic efflux events of varying magnitude and spatial distribution, irrespective of variations in barometric pressure and soil water content, over the course of the active injection (Forde et al., 2018). These gas emission dynamics were not readily evident in our simulations which indicates that a variety of other subsurface factors (e.g., small-scale heterogeneity, water table fluctuations) are potentially acting in combination with changes in the leakage rate.

3.8 Injector Configuration

To examine the impact of two simultaneous injectors on the spatiotemporal evolution of the gas plume, three cases using the actual injection rate history in a uniform aquifer were employed: one case using only the shallow injector; one case using only the deep injector; and one case using both injectors. At Day 71 (Figure 10), the shallow injector case formed a broad, nearly symmetrical plume, while the deeper injector formed a narrower and less symmetric plume that preferentially migrated down-gradient. When both injectors were used simultaneously, the gas distribution resembled a superposition of the gas distributions from the individual injectors;

however, both lateral spreading above the shallow injector and the extension of the plume down-gradient were enhanced relative to the individual cases.

The distribution of gas shown in Figure 10 exemplifies the effect of counteracting forces between buoyancy and hydrostatic pressure during methane injection. When gas is injected near the surface alone (i.e., 4.5 m bgs) the gas spreads equally far up- and down-gradient, whereas gas from the deeper well alone migrated almost entirely down-gradient of the injection point. For the latter case, gas migration was heavily influenced by pressure head gradients. Forde et al. (in press) also noted drastic changes in the concentration of methane gas in the vadose zone and efflux rates to atmosphere during Phase III, when the shallow injector was temporarily turned off. The broader gas plume simulated around the shallow injector together with the field observations indicates that methane migration will be strongly controlled by the depth of the leakage point within the aquifer.

4.0 Conclusions

Our multi-phase flow modelling based on data collected during a field injection experiment by Cahill et al. (2017) showed that the evolution of a gas-phase plume would be variably impacted by changes in permeability, anisotropy, groundwater velocity, layer thickness, and geometrical properties of the aquifer and injector configuration, with more marked impacts associated with anisotropy, changes in gas-entry entry pressure of lower permeability layers within the aquifer, and injection rate history. Without changes in entry pressure between two layers, gas-phase accumulations typically did not exhibit sharp changes in saturation. Although this had a minimal impact on gas retention in the aquifer, entry pressure variations had a marked impact on the gas phase distribution.

The simulated behaviour of gas injected under a layer with increased layer entry pressure scenarios are more consistent with previous immiscible-phase field experiments which show pooling of fluids along permeability contrasts. For instance, when entry pressure changes are present between two layers, the gas accumulates along the boundary and forms laterally extensive pools. Once gas reaches a pressure higher than the entry pressure of the confining layer or when a discontinuity is reached, the gas migrates upwards via buoyancy resulting in a series of gas migration hotspots effluxing to the vadose zone, which is consistent with the field experiment. The characteristics of vertical preferential pathways and gas hotspots at the water table depended primarily on the severity of the permeability contrast, entry pressure variations, and layer discontinuities; although less dominant factors such as groundwater velocity and injection configuration also contributed to the formation of hotspots.

Numerical simulations showed that the inclusion of vertical permeability barriers to flow (e.g., vertical permeability contrasts, increasing layer thickness, and anisotropy) or a component of horizontal groundwater flow will increase gas retention within the aquifer compared to a more uniform or weakly anisotropic scenario (i.e., 4 – 5 m^3 vs. 2 m^3 at residual gas saturation). The temporary shut-down in gas injection was also shown to influence the rate of gas saturation simply based on the rate of gas retained in the aquifer before the temporary shut-down and immediately after injection commenced. Therefore, perturbations in the source zone pressure will likely lead to more complex gas-phase distributions and residence times within an aquifer.

Insights gained through these numerical flow simulations were generally consistent with the interpreted methane migration and behaviour in the unconfined shallow aquifer experiment (e.g., Cahill et al., 2017; Steelman et al., 2017; Cahill et al., 2018). Our models show that subtle depositional variations within a homogeneous aquifer comprised of a series of anisotropic thin

sand lenses of varying permeability and gas-entry pressures would result in a laterally intensive gas-phase plume. The field experiment and numerical simulations both showed that a portion of the injected methane escaped to the atmosphere while the remainder accumulated in the subsurface. While the field experiment showed that changes in the methane injection rate, particularly a temporary shut-down of the injection, would markedly affect the migration of the methane to the vadose zone, perturbations in its lateral extent combined with rapid accumulation and dissipation of gas within the aquifer were not replicated in the numerical models (Steelman et al., 2017; Cahill et al., 2018). Therefore, the gas plume dynamics observed during the field experiment are most likely being enhanced through external processes (e.g., recharge, barometric/hydraulic pressure variations, and temperature) combined with more heterogeneous flow property distributions leading to spatiotemporal variations in hydrostatic pressure.

This modelling was completed under the assumption that the bulk hydraulic properties of soil would adequately describe the movement of methane gas in the aquifer over the relatively short time scale of the injection experiment. Although the scenarios were simplistic, they demonstrate the importance of heterogeneity (i.e., layers with variable permeability and capillary pressure) on the evolution of a methane gas plume emanating from a pair of point sources. Here, the lateral extent of gas migration relative to the depth of the injection was quite substantial (2 – 3 times the depth). Other numerical simulations of wellbore leakage in an unconfined aquifer by Roy et al. (2016) suggest that gas will migrate upwards due to buoyancy along the well casing, without being shunted laterally, and eventually escape to the atmosphere. If the well-bore casing is not fully compromised (i.e., it remains partially sealed to vertical leakage, then it is reasonable to conclude that methane will most likely migrate laterally along permeability boundaries as demonstrated by Cahill et al. (2017) and Steelman et al. (2018). Our numerical study reaffirms

the propensity for methane gas to migrate horizontally from leaking hydrocarbon production wells even in relatively uniform aquifers, resulting in more complex groundwater contaminant plumes than those depicted by previous numerical investigations of deeper groundwater systems (e.g., Rice et al., 2018).

Deep sedimentary basins where petroleum resources are typically exploited exhibit significant heterogeneity and anisotropy. Consequently, it should be anticipated that during subsurface leakage of natural gas from a point source in such groundwater systems that a significant portion or even potentially all fugitive gas might be retained in the aquifer and transported laterally assuming enough permeability barriers are encountered. Depending on the nature of the gas barriers or traps that impede vertical flow, the gas may travel far from the well bore and may not reach the surface. Hence, not all energy wells exhibiting subsurface gas migration will be identified by surficial monitoring and soil gas surveys around the well head; methods most commonly used to detect leakage (Forde et al., 2019). This work highlights the importance of lateral migration due to typical layering in sediment deposits and the need for robust monitoring and detection programs for gas migration and fugitive gas into the fresh groundwater zones located substantial distances from energy wells.

Acknowledgements

This research was made possible through an NSERC Strategic Partnerships Grant Project (SPG-P) awarded to Drs John Cherry and Beth Parker along with their project collaborators Drs. Bernhard Mayer, Ulrich Mayer and Cathryn Ryan. The authors would like to thank Dr. Andre Unger for his technical support and guidance on the use of CFbio, and three anonymous reviewers for their thoughtful and constructive feedback.

References

Brewster, M.L., Annan, A.P., Greenhouse, J.P., Kueper, B.H., Olhoeft, G.R., Redman, J.D., Sander, K.A., 1995. Observed migration of a controlled DNAPL release by geophysical methods. Groundwater 33, 977–987.

Broholm, K., Feenstra, S., Cherry, J.A., 1999. Solvent release into a sandy aquifer: 1. Overview of source distribution and dissolution behavior. Environ. Sci. Technol. 33, 681–690.

Cahill, A.G., Parker, B.L., Mayer, B., Mayer, K.U., Cherry, J.A., 2018. High resolution spatial and temporal evolution of dissolved gases in groundwater during a controlled natural gas release experiment. Sci. Total Environ. 622-623, 1178–1192. doi:10.1016/j.scitotenv.2017.10.049

Cahill, A.G., Steelman, C.M., Forde, O., Kuloyo, O., Ruff, E., Mayer, B., Mayer, K.U., Strous, M., Ryan, M.C., Cherry, J.A., Parker, B.L., 2017. Mobility and persistence of methane in groundwater in a controlled release field experiment. Nat. Geosci.10, 289–294. doi:10.1029/2007JG000575.

Das, B.M., 2008. Advanced Soil Mechanics (3rd edition). New York, NY. doi: 10.1029/EO066i042p00714-02.

Eltschlager, K.K., Hawkins, J.W., Ehler, C., Baldassare, F., 2001. *Technical measures for the Investigation and Mitigation of Fugitive Methane Hazards in Areas of Coal Mining* (US Department of the Interior, Office of Surface Mining Reclamation and Enforcement, Pittsburgh).

Forde, O.N., Mayer, K.U., Cahill, A.G., Mayer, B., Cherry, J.A., Parker, B.L., 2018. Vadose zone gas migration and surface effluxes following a controlled natural gas release into an unconfined shallow aquifer. Vadose Zone J. 17, 180033. doi: 10.2136/vzj2018.02.0033.

Forde, O.N., Mayer, K.U., Hunkeler, D., 2019. Identification, spatial extent and distribution of fugitive gas migration on the well pad scale. Sci. Total Environ. 652, 356–366. doi: 10.1016/j.scitotenv.2018.10.217

Forsyth, P. A., Shao, B. Y., 1991. Numerical simulation of gas venting for NAPL site remediation. Adv. Water Resour. 14, 354–367.

Jackson, R.B., Vengosh, A., Darrah, T.H., Warner, N.R., Down, A., Poreda, R.J., Osborn, S.G., Zhao, K.G., Karr, J.D., 2013. Increased stray gas abundance in a subset of drinking water wells near Marcellus shale gas extraction. Proc. Natl. Acad. Sci. U. S. A. 110, 11250–11255. doi: 10.1073/pnas.1221635110

Kelly, W.R., Matisoff, G., Fisher, J.B., 1985. The effects of a gas-well blow-out on groundwater chemistry. Environ. Geol. Water Sci. 7, 205–213.

Kueper, B.H., Frind, E.O., 1991. Two-phase flow in heterogeneous porous media: 2. Model application. J. Contam. Hydrol. 2, 95–110.

Kueper, B.H., Redman, D., Starr, R.C., Reitsma, S., Mah, M., 1993. A field experiment to study the behaviour of tetrachloroethylene below the water table: Spatial distribution of residual and pooled DNAPL. Groundwater 31, 756–766.

Laukonen, K.A., Parker, B.L., Cherry, J.A., 2000. Internal characteristics of a bromide tracer zone during natural flow in the Borden aquifer, Ontario, Canada. Tracers and Modelling in Hydrogeology. In: Proceedings of TraM'2000 Conference. 262. IAHS Publication, Liege, Belgium, pp. 227–233.

Malakoff, D., 2014. The gas surge. Science 344, 1464–1467.

Moortgat, J., Schwartz, F.W., Darrah, T.H., 2018. Numerical modeling of methane leakage from a faulty natural gas well into fractured tight formations. Groundwater, 1–13. doi: 10.1111/gwat.12630

Osborn, S.G., Vengosh, A., Warner, N.R., Jackson, R.B., 2011. Methane contamination of driking water accompanying gas-well drilling and hydraulic fracturing. Proc. Natl. Acad. Sci. U. S. A. 108, E665–E666. doi: 10.1073/pnas.1109270108.

Perrodon, A., 1983. Dynamics of oil and gas accumulations. Pau, France: Elf Aquitaine.

Rice, A.K., McCray, J.E., Singha, K., 2018. Methane leakage from hydrocarbon wellbores into overlying groundwater: Numerical investigation of multiphase flow processes governing migration. Water Resour. Res. 54, doi: 10.1002/2017WR021365

Roy, N., Molson, J., Lemieux, J.-M., Van Stempvoort, D., Nowamooz, A., 2016. Three-dimensional numerical simulations of methane gas migration from decommissioned hydrocarbon production wells into shallow aquifers. Water Resour. Res. 52, 5598–5618. doi: 10.1002/2016WR018686.

Schout, G., Hartog, N., Hassanizadeh, S.M., Griffioen, J., 2018. Impact of an historic underground gas well blowout on the current methane chemistry in a shallow groundwater system. Proc. Natl. Acad. Sci. U. S. A. 115, 296–301. doi: 10.1073/pnas.1711472115.

Sudicky, E.A., Illman, W.A., 2011. Lessons learned from a suite of CFB Borden Experiments. Groundwater 49, 630–648. doi: 10.1111/j.1745-6584.2011.00843.x

Steelman, C.M., Klazinga, D.R., Cahill, A.G., Endres, A.L., Parker, B.L., 2017. Monitoring the evolution and migration of a methane gas plume in an unconfined sandy aquifer using time-lapse GPR and ERT. J. Contam. Hydrol. 205, 12 – 24. doi:10.1016/j.jconhyd.2017.08.011

Thomson, D.A., 2004. Influence of grain size variability and sedimentology on solvent DNAPL distribution in the Borden aquifer. MSc Thesis. University of Waterloo, Waterloo.

Thomson, N.R., Johnson, R.L., 2000. Air distribution during in situ air sparging: an overview of mathematical modeling. J. Hazard. Mater. 72, 265–282.

Tomlinson, D.W., Thomson, N.R., Johnson, R.L., Redman, J.D., 2003. Air distribution in the Borden aquifer during in situ air sparging. J. Contam. Hydrol. 67, 113 – 132. doi:10.1016/S0169-7722(03)00070-6.

Unger, A. J. A., Sudicky, E. A., & Forsyth, P. A. (1995). Mechanisms Controlling Vacuum Extraction Coupled with Air Sparging for Remediation of Heterogeneous Formations Contaminated by Dense Nonaqueous Phase Liquids. Water Resour. Res., 31, 1913– 1925.

Walton, K.M., Unger, A.J.A., Ioannidis, M.A., Parker, B.L. 2017. Impact of eliminating fracture intersection nodes in multiphase compositional flow simulation. Water Resour. Res., 53, 2917-2939, doi: 10.1002/2016WR020088.

Walton, K., Unger, A., Ioannidis, M., Parker, B., Benchmarking NAPL redirection and matrix entry at fracture intersections below the water table. Water Resour. Res., doi: 10.1029/2018WR023435.

Table 1. Methane injection rates and approximate periods for the field experiment (*from* Cahill et al. 2018).

Phase	Injection Period		Injection Rates	
	start	*end*	*shallow*	*deep*
	days		L/min	
I	0	28	0.06	0.06
II[1]	28	68	0.35	0.35
III	68	70	0.00	0.35
IV	70	72	1.50	1.50
V	72	-	scheduled shut down	

[1]an unscheduled shutdown of the injection system occurred between days 39 – 43.

Table 2. Parameters for the base case and sensitivity analysis

Property	Value	Modelled Range
Hydraulic Properties		
Aquifer permeability[1]	2.2×10^{-12} m^2	1.2×10^{-12} m^2 – 6.6×10^{-13} m^2
Aquifer porosity	0.33	-
Aquitard permeability	6.4×10^{-14} m^2	6.4×10^{-14} m^2
Aquitard porosity	0.39	-
Anisotropy ratio (k_h/k_v)	10	5 – 30
Groundwater velocity	6 cm/day	0 cm/day – 10 cm/day
Entry pressure[2]	2.22 kPa	2.22 kPa, 2.99 kPa
Residual saturation[2]	0.078	-
Pore size distribution index[2]	2.48	-
Residual gas saturation	0.1	-
Geometric Properties		
Depth to layer	3 m	-
Layer thickness	0.5 m	0.2 m – 1.0 m
Layer discontinuity	1 m	-1.5, 2.5, 6.5 m

Aquitard depth	9 m	-
Depth to water table	1 m	-
Model length	20 m	-
Model depth	10 m	-
Model discretization	0.1 m	-
Injector properties		
Upper injector depth	4.5 m	-
Lower injector depth	9.0 m	-

[1]values were varied for the layer embedded within the aquifer.

[2]Brooks and Corey (1964) model parameters from Kueper and Frind (1991).

Table 3. Physical parameters for sensitivity analysis.

Scenarios	Parameters	Description
Permeability (varying layer permeability)	$k_L = 1 \times k_{aq}$ $k_L = 0.55 \times k_{aq}$ $k_L = 0.3 \times k_{aq}$ $k_L = 0.1 \times k_{aq}$ $k_L = 0.03 \times k_{aq}$	A uniform aquifer (i.e., $k_{aq} = 2.2 \times 10^{-12}$ m^2, $\phi = 0.33$) with and without a layer (from 3.0 m – 3.5 m bgs, $\phi = 0.33$)
Anisotropy	$k_h/k_v = 5$ $k_h/k_v = 10$ $k_h/k_v = 30$	A uniform aquifer and an aquifer with a layer ($k_{h,L} = 0.1 \times k_{aq}$, $\phi = 0.33$) from 3.0 m – 3.5 m each with adjusted k_v values
Groundwater Velocity	0 cm/day 3 cm/day 6 cm/day 10 cm/day	A uniform aquifer with varying groundwater velocity
Layer Thickness	0.2 m 0.5 m 1.0 m	A uniform aquifer containing a layer with $k_L = 0.55 \times k_{aq}$ and $\phi = 0.33$ of varying thicknesses
Layer Entry Pressure	2.22 kPa 2.99 kPa	A uniform aquifer containing a layer from 3.0 m – 3.5 m with $k_L = 0.55 \times k_{aq}$ and $\phi = 0.33$ with varying entry pressure
Centre of Discontinuity	-1.5 m 2.5 m 6.5 m	A uniform aquifer containing a layer ($k_L = 0.55 \times k_{aq}$, $\phi = 0.33$ and $P_c = 2.99$ kPa) with a 1 m wide discontinuity centered at different points along the model domain
Injection Rate History	Actual Injection History Constant 0.006 L/min Constant 0.35 L/min Constant 1.50 L/min	A uniform aquifer and an aquifer with a layer from 3.0 m – 3.5 m bgs ($k_L = 0.1 \times k_{aq}$, $\phi = 0.33$) using different injection rate histories
Injection Configuration	Shallow only Deep only Both	A uniform aquifer using different injector configurations with the actual injection history

Figure 1. Geometry of the 2D base case model domain consisting of a homogeneous anisotropic aquifer overlying an aquitard with two gas injectors positioned at 4.5 m and 9.0 m bgs (after Cahill et al., 2017). The water table is positioned at 1 m bgs directly above the injection points. Groundwater flow occurs from left to right.

Figure 2. Simulated gas injection rate history based on Cahill et al. (2017). A total of 48.7584 m^3 of methane gas was injected into the aquifer during each simulation.

Figure 3. a) Gas saturation on Day 56 for five cases with differing permeability contrasts between the layer (k_L) and aquifer (k_{aq}) for the same horizontal groundwater velocity (arrows: v = 6 cm/day). Note the formation of gas hotspots (H) at the water table interface. The pre-injection water table is shown by the grey dashed line; the injectors by white circles; the aquitard by the grey cross-hatching and the lower permeable layer by the grey single hatched area. b) Total volume of gas in the subsurface for the five permeability contrast cases at standard temperature and pressure over the full 102 day simulation period.

Figure 4. a) Gas saturation on Day 56 for three cases with different anisotropy (k_h/k_v) for a uniform aquifer with no layer, and an aquifer with a layer. Note the formation of gas hotspots (H) at the water table interface. The pre-injection water table is shown by the grey dashed line; the injectors by white circles; the aquitard by the grey cross-hatching and the lower permeable layer by the grey single hatched area b) Total volume of gas in the subsurface for each model case at standard temperature and pressure over the full 102 day simulation period.

Figure 5. Gas saturation on Day 56 for four cases with differing groundwater velocity in a uniform aquifer. Note the formation of gas hotspots (H) at the water table interface. The pre-injection water table is shown by the grey dashed line; the injectors by white circles; the aquitard by the grey cross-hatching. b) Total volume of gas in the subsurface for the four velocity cases at standard temperature and pressure over the full 102 day simulation period.

Figure 6. Gas saturation on Day 56 for three cases with differing layer thickness. Note the formation of gas hotspots (H) at the water table interface. The pre-injection water table is shown by the grey dashed line; the injectors by white circles; the aquitard by the grey cross-hatching and the lower permeable layer by the grey single hatched area. b) Total volume of gas in the subsurface for the three layer thickness cases at standard temperature and pressure over the full 102 day simulation period.

Figure 7. a) Gas saturation on Days 20, 37 and 56 for two cases with differing entry pressures (P_c = 2.22 kPa and 2.99 kPa); the permeability of the layer was set to $k_L = 0.55 \times k_{aq.}$ Note the formation of gas hotspots (H) at the water table interface. The pre-injection water table is shown by the grey dashed line; the injectors by white circles; the aquitard by the grey cross-hatching; and the lower permeable layer by the grey single hatched area. b) Total volume of gas in the subsurface for the three layer thickness cases at standard temperature and pressure over the full simulation period.

Figure 8. a) Gas saturation on Day 56 for three cases with a 1 m discontinuity in the layer (k_L = $0.55 \times k_{aq,}$ $\phi = 0.33$ and P_c = 2.99 kPa). Note the formation of gas hotspots (H) at the water table interface. The pre-injection water table is shown by the grey dashed line; the injectors by white circles; the aquitard by the grey cross-hatching; and the lower permeable layer by the grey single

hatched area. b) Total volume of gas in the subsurface for the three layer discontinuity cases at standard temperature and pressure over the full simulation period.

Figure 9. Total volume of gas in the subsurface at standard temperature and pressure for four cases with differing gas injection rates in a uniform aquifer with a layer between 3.0 and 3.5 mbgs with $k_L = 0.55 \times k_{aq}$.

Figure 10. Gas saturation on Day 71 for three cases of a uniform aquifer using the actual injection rate history with only the shallow and deep injections, and both injectors simultaneously. The pre-injection water table is shown by the grey dashed line; the injectors by white circles; the aquitard by the grey cross-hatching.

Highlights

- Numerical simulations were used to investigate CH_4 migration in an unconfined aquifer
- Numerical models were based on a controlled CH_4 injection experiment at CFB Borden
- 2D simulations assessed importance of hydraulic parameters and flow system conditions
- Subtle permeability and capillary pressure contrasts led to extensive lateral gas migration
- CH_4 travelled much farther and faster than that predicted by groundwater advection

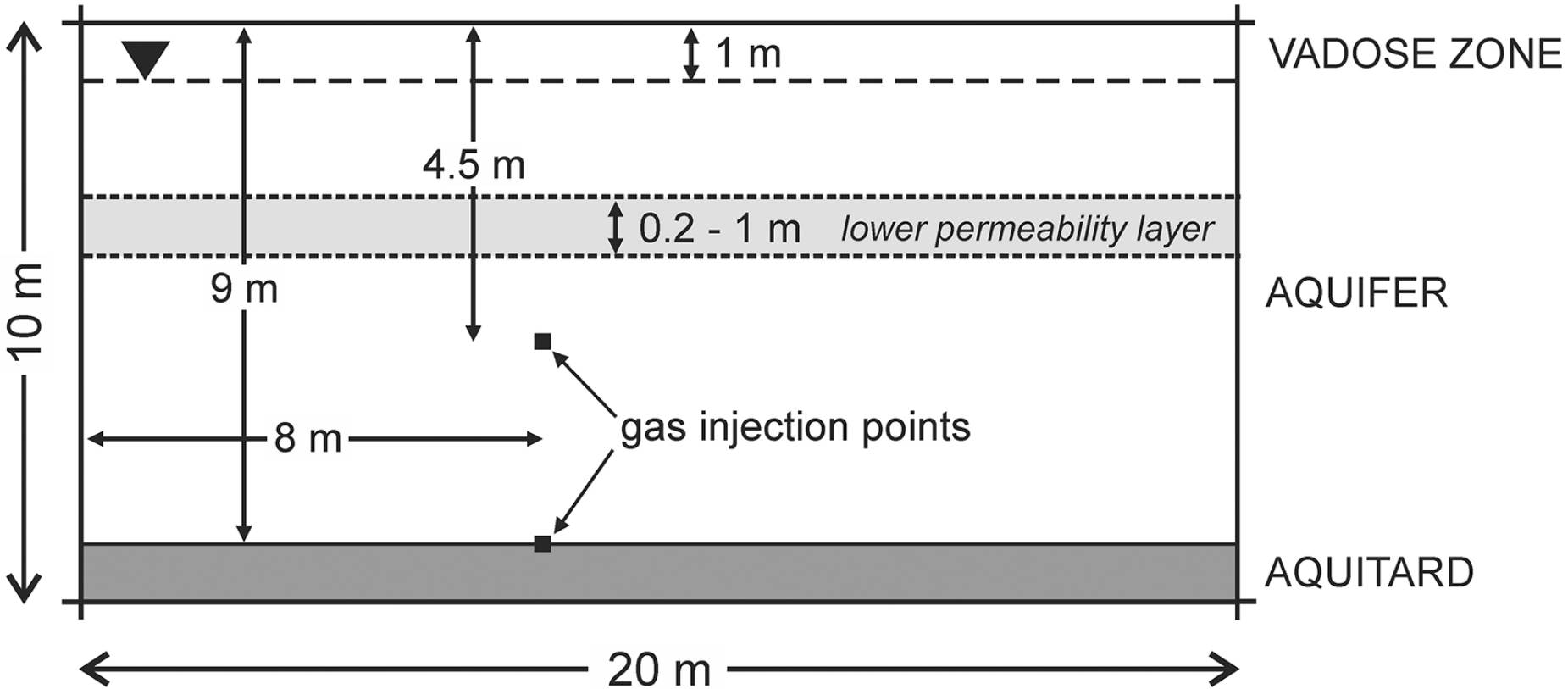
1 m
VADOSE ZONE
4.5 m
0.2 - 1 m
lower permeability layer
9 m
AQUIFER
10 m
8 m
gas injection points
AQUITARD
20 m

Figure 1

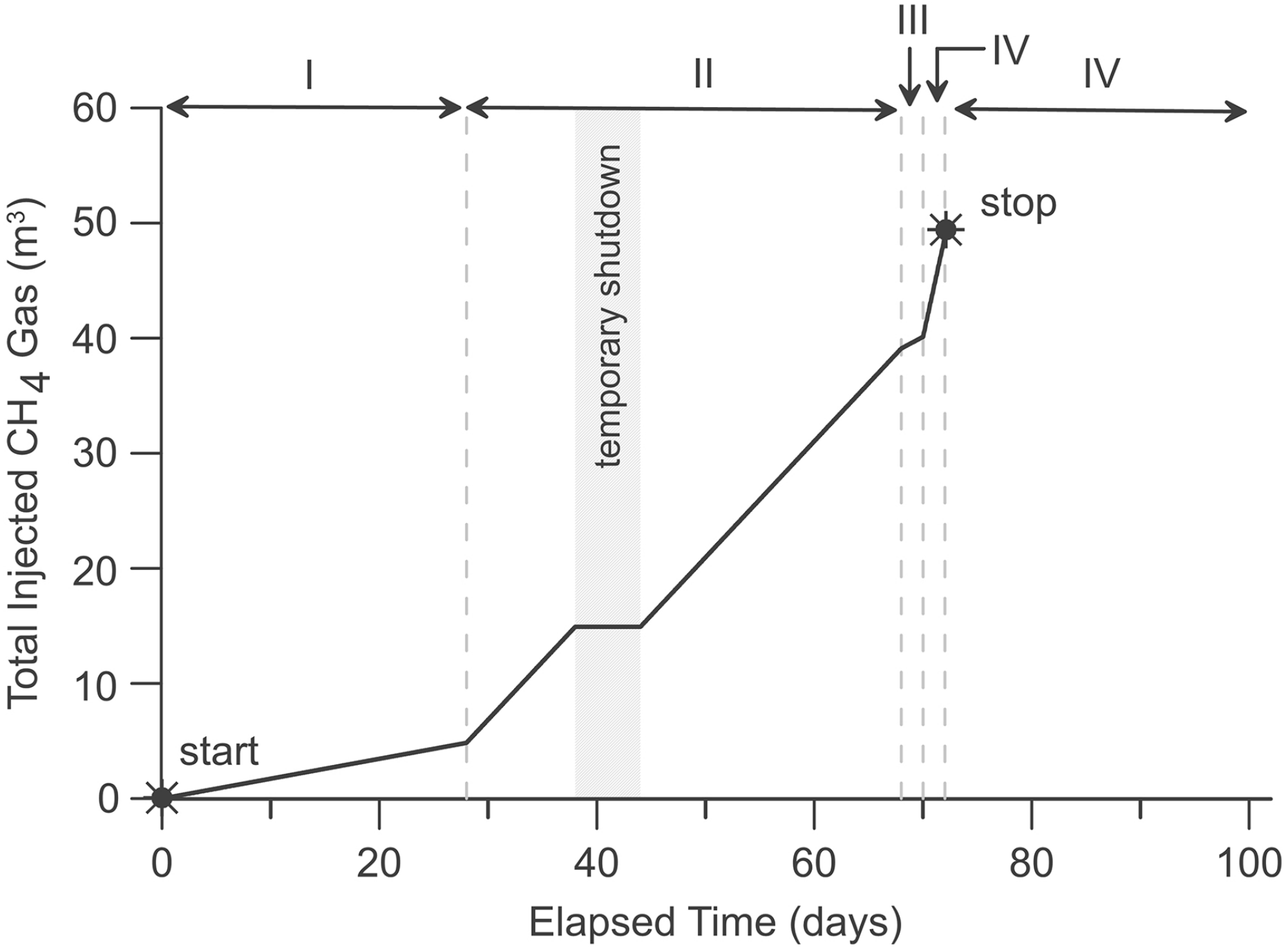
I
II
III
IV
IV
temporary shutdown
stop
start
Total Injected CH_4 Gas (m^3)
0
10
20
30
40
50
60
0
20
40
60
80
100
Elapsed Time (days)

Figure 2

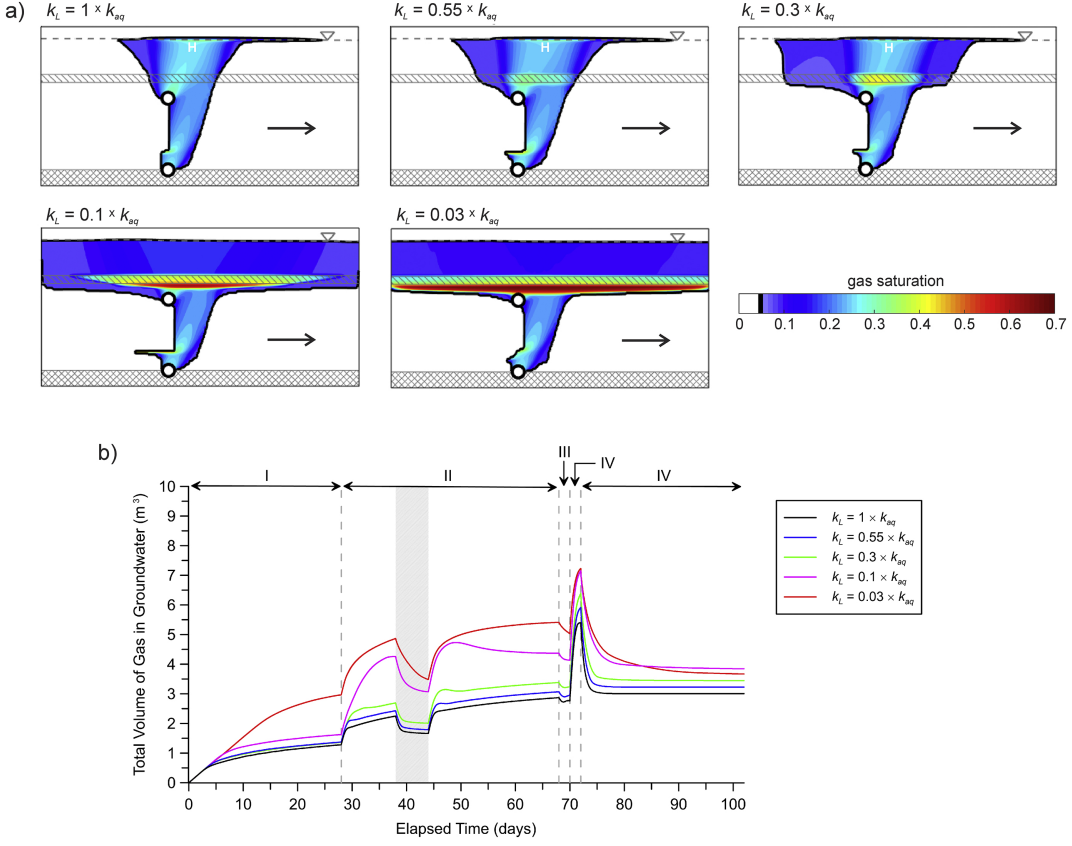
a)
$k_L = 1 \times k_{aq}$
$k_L = 0.55 \times k_{aq}$
$k_L = 0.3 \times k_{aq}$
$k_L = 0.1 \times k_{aq}$
$k_L = 0.03 \times k_{aq}$
H
gas saturation
0 0.1 0.2 0.3 0.4 0.5 0.6 0.7
b)
I
II
III
IV
IV
Total Volume of Gas in Groundwater (m^3)
Elapsed Time (days)
0 10 20 30 40 50 60 70 80 90 100
0 1 2 3 4 5 6 7 8 9 10
$k_L = 1 \times k_{aq}$
$k_L = 0.55 \times k_{aq}$
$k_L = 0.3 \times k_{aq}$
$k_L = 0.1 \times k_{aq}$
$k_L = 0.03 \times k_{aq}$

Figure 3

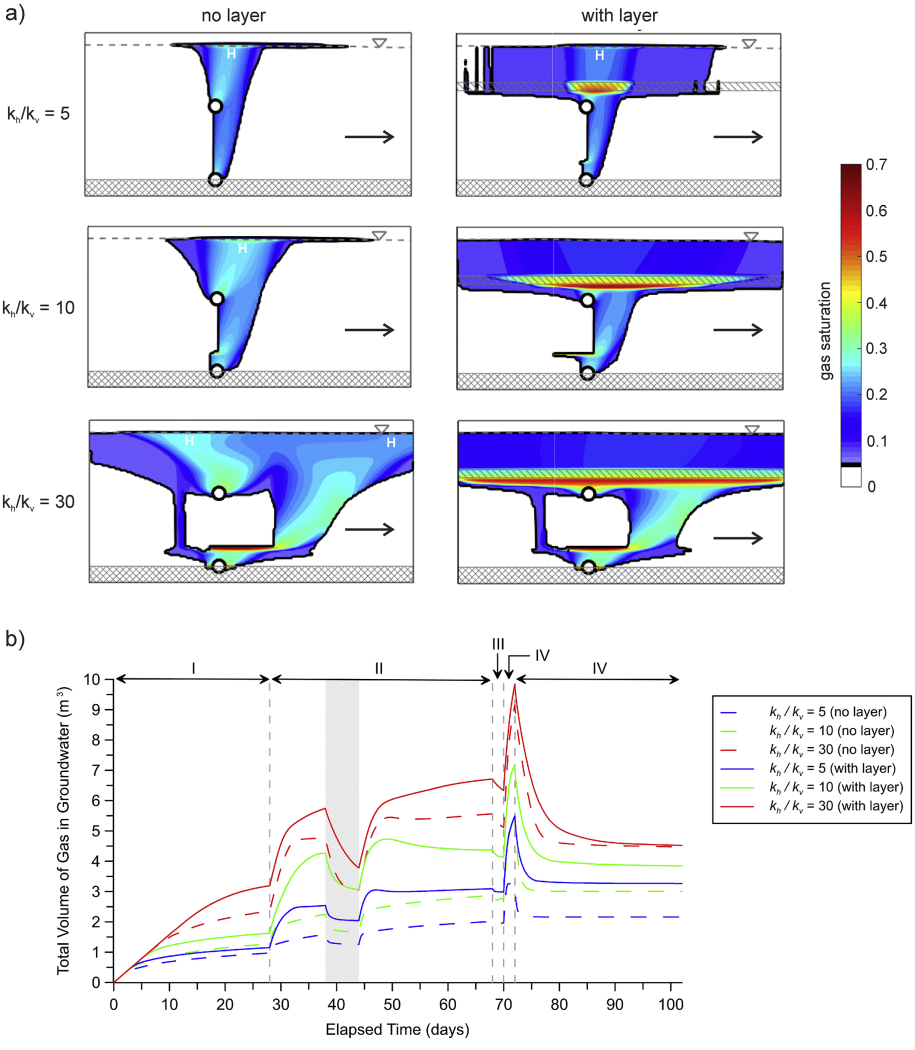
a)
no layer
with layer
k_h/k_v = 5
k_h/k_v = 10
k_h/k_v = 30
H
gas saturation
0.7
0.6
0.5
0.4
0.3
0.2
0.1
0
b)
I
II
III
IV
IV
Total Volume of Gas in Groundwater (m^3)
Elapsed Time (days)
k_h / k_v = 5 (no layer)
k_h / k_v = 10 (no layer)
k_h / k_v = 30 (no layer)
k_h / k_v = 5 (with layer)
k_h / k_v = 10 (with layer)
k_h / k_v = 30 (with layer)

Figure 4

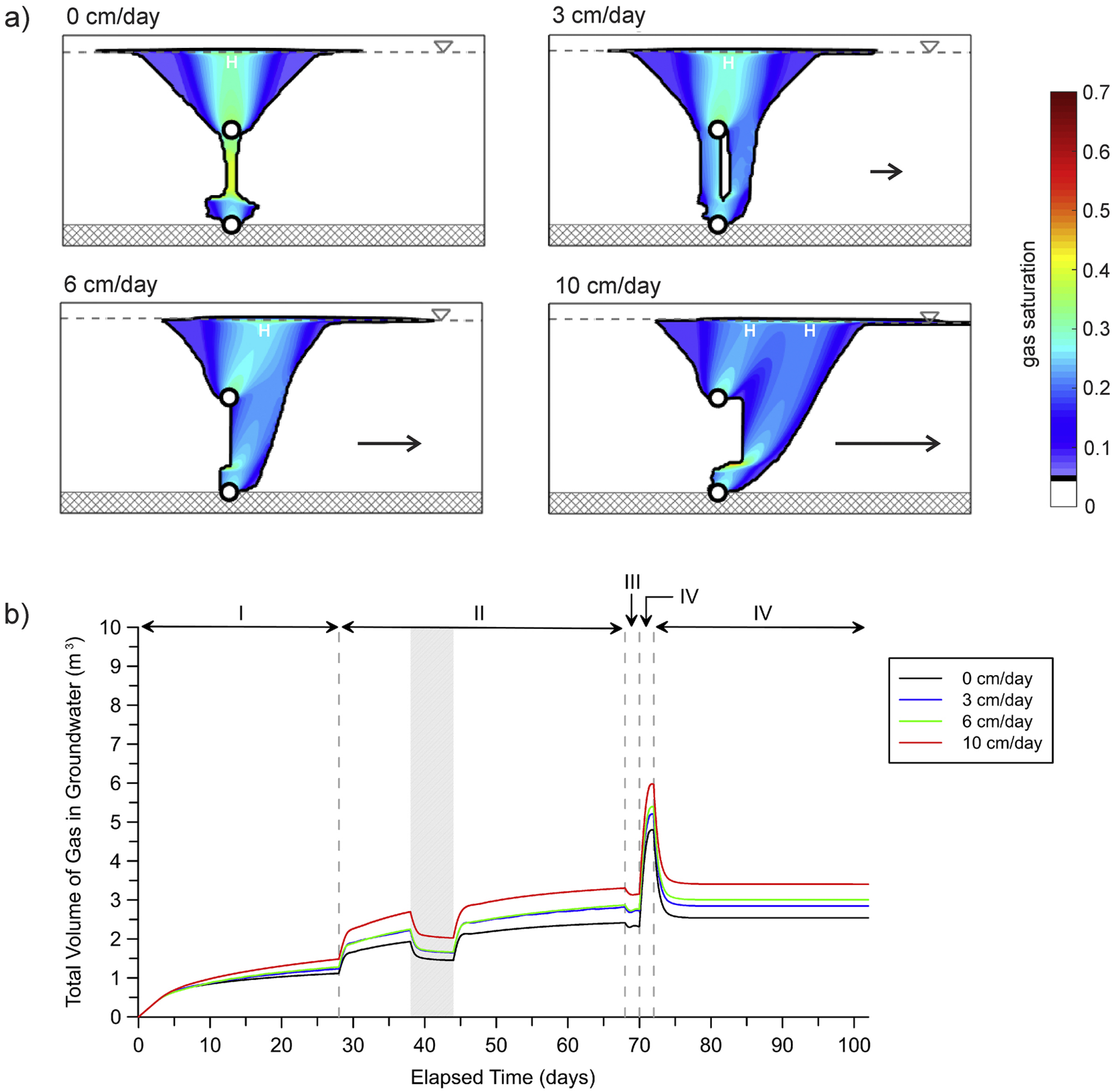
a)
0 cm/day
3 cm/day
6 cm/day
10 cm/day
H
gas saturation
0.7
0.6
0.5
0.4
0.3
0.2
0.1
0
b)
I
II
III
IV
IV
Total Volume of Gas in Groundwater (m3)
Elapsed Time (days)
0 cm/day
3 cm/day
6 cm/day
10 cm/day

Figure 5

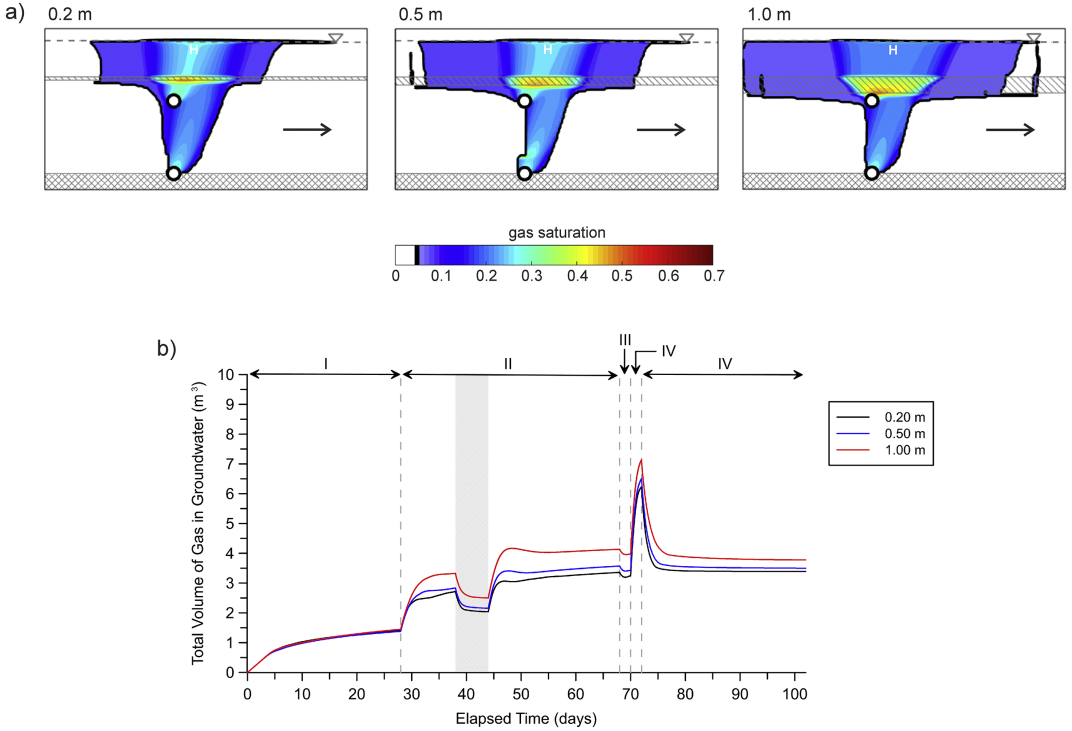
a)
0.2 m
0.5 m
1.0 m
H
gas saturation
0
0.1
0.2
0.3
0.4
0.5
0.6
0.7
b)
I
II
III
IV
IV
Total Volume of Gas in Groundwater (m3)
Elapsed Time (days)
0.20 m
0.50 m
1.00 m

Figure 6

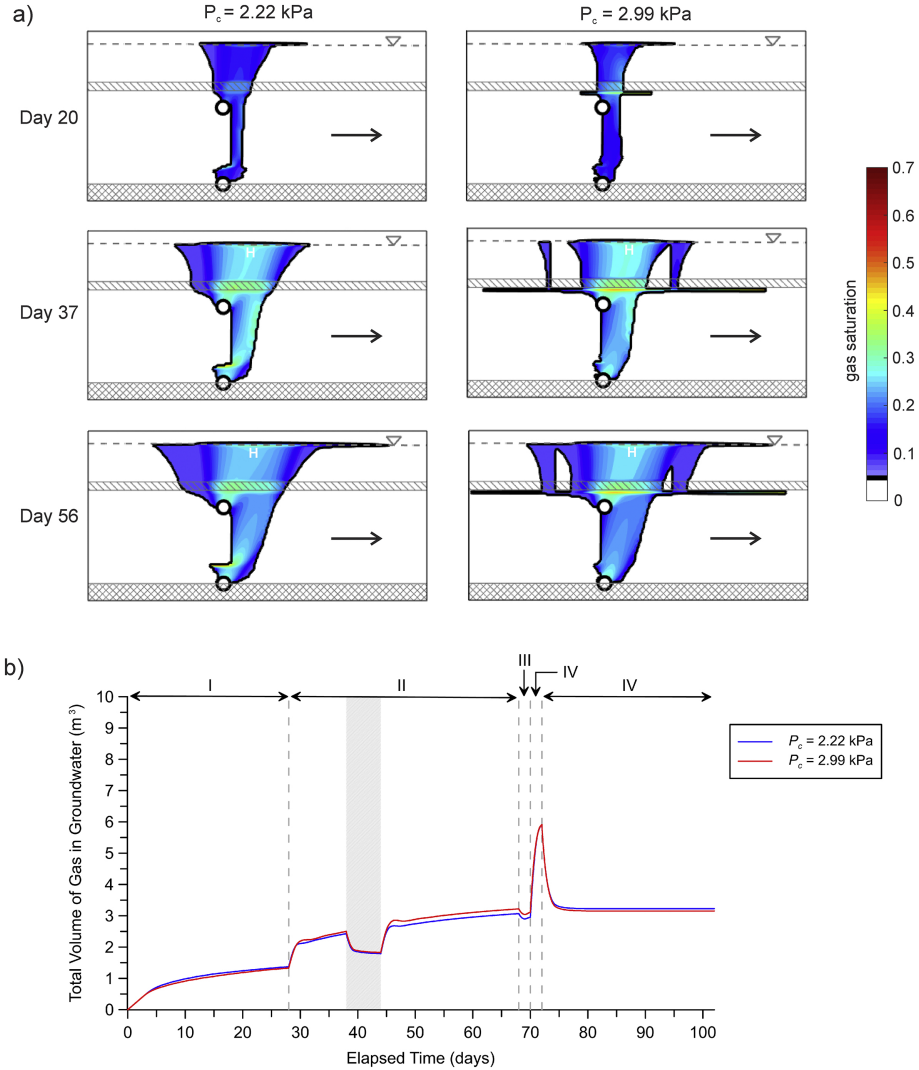
a)
P_c = 2.22 kPa
P_c = 2.99 kPa
Day 20
Day 37
Day 56
H
gas saturation
0.7
0.6
0.5
0.4
0.3
0.2
0.1
0
b)
I
II
III
IV
IV
Total Volume of Gas in Groundwater (m³)
Elapsed Time (days)
P_c = 2.22 kPa
P_c = 2.99 kPa
0
1
2
3
4
5
6
7
8
9
10
0
10
20
30
40
50
60
70
80
90
100

Figure 7

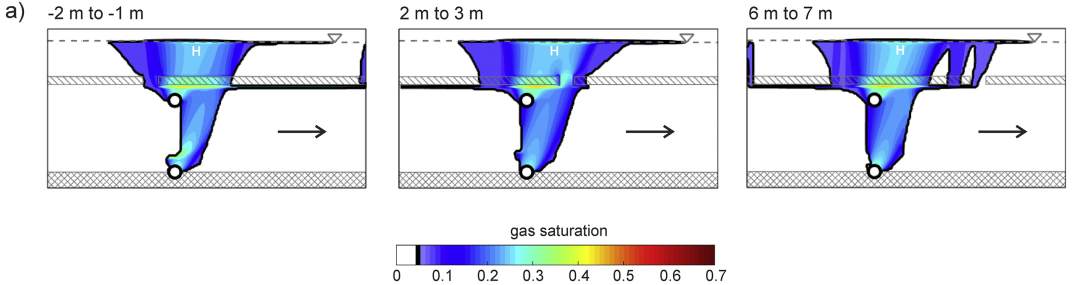
a)
-2 m to -1 m
2 m to 3 m
6 m to 7 m
H
gas saturation
0
0.1
0.2
0.3
0.4
0.5
0.6
0.7

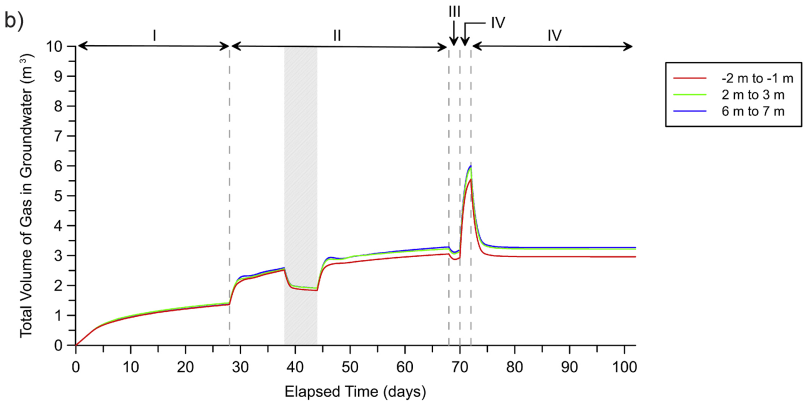
b)
I
II
III
IV
IV
Total Volume of Gas in Groundwater (m3)
Elapsed Time (days)
-2 m to -1 m
2 m to 3 m
6 m to 7 m

Figure 8

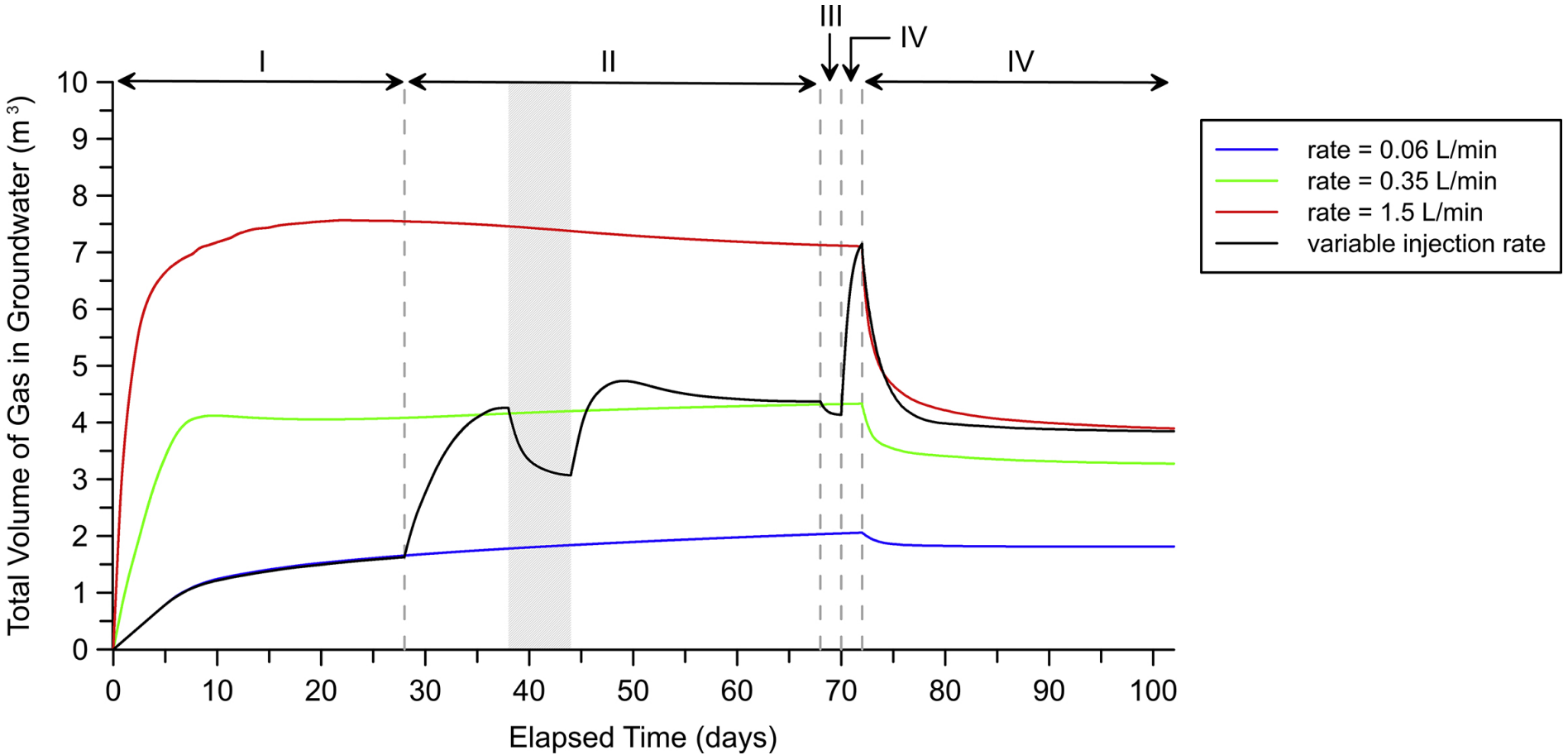
I
II
III
IV
IV
Total Volume of Gas in Groundwater (m³)
Elapsed Time (days)
0
1
2
3
4
5
6
7
8
9
10
0
10
20
30
40
50
60
70
80
90
100
rate = 0.06 L/min
rate = 0.35 L/min
rate = 1.5 L/min
variable injection rate

Figure 9

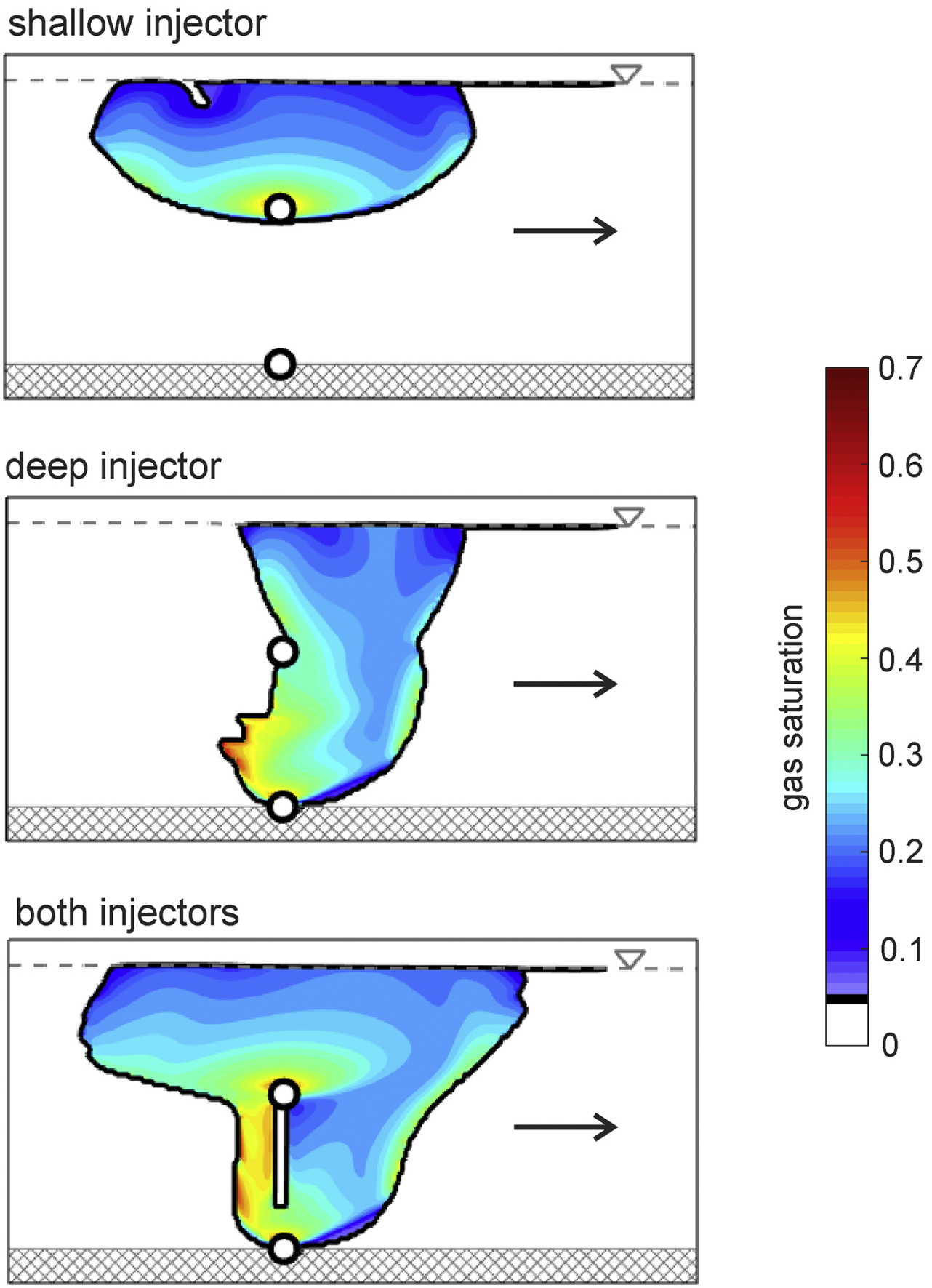
shallow injector
deep injector
both injectors
gas saturation
0.7
0.6
0.5
0.4
0.3
0.2
0.1
0

Figure 10